Ability of phages to infect *Acinetobacter calcoaceticus-Acinetobacter baumannii* complex species through acquisition of different pectate lyase depolymerase domains

Hugo Oliveira,[1][†] Ana R. Costa,[1][†]
Nico Konstantinides,[1,2] Alice Ferreira,[1]
Ergun Akturk,[1] Sanna Sillankorva,[1]
Alexandr Nemec,[3] Mikhail Shneider,[4]
Andreas Dötsch[5,6] and Joana Azeredo[1]*

[1]*CEB – Centre of Biological Engineering, LIBRO – Laboratório de Investigação em Biofilmes Rosário Oliveira, University of Minho, 4710-057 Braga, Portugal.*
[2]*Laboratory of Microbiology, Wageningen University, Stippeneng, 6708 WE Wageningen, The Netherlands.*
[3]*Laboratory of Bacterial Genetics, National Institute of Public Health, Šrobárova 48, 100 42 Prague, Czech Republic.*
[4]*Laboratory of Molecular Bioengineering, 16/10 Miklukho-Maklaya St, Shemyakin-Ovchinnikov Institute of Bioorganic Chemistry, 117997 Moscow, Russia.*
[5]*Institute of Functional Interfaces, Karlsruhe Institute of Technology (KIT), Eggenstein-Leopoldshafen, Germany.*
[6]*Max Rubner-Institute, Institute for Physiologie and Biochemistry of Nutrition, Haid-und-Neu-Str. 9, 76131 Karlsruhe, Germany.*

Summary

Bacteriophages are ubiquitous in nature and represent a vast repository of genetic diversity, which is driven by the endless coevolution cycle with a diversified group of bacterial hosts. Studying phage-host interactions is important to gain novel insights into their dynamic adaptation. In this study, we isolated 12 phages infecting species of the *Acinetobacter baumannii-Acinetobacter calcoaceticus* complex which exhibited a narrow host range and similar morphological features (podoviruses with short tails of 9–12 nm and isometric heads of 50–60 nm). Notably, the alignment of the newly sequenced phage genomes (40–41 kb of DNA length) and all *Acinetobacter* podoviruses deposited in Genbank has shown high synteny, regardless of the date and source of isolation that spans from America to Europe and Asia. Interestingly, the C-terminal pectate lyase domain of these phage tail fibres is often the only difference found among these viral genomes, demonstrating a very specific genomic variation during the course of their evolution. We proved that the pectate lyase domain is responsible for phage depolymerase activity and binding to specific *Acinetobacter* bacterial capsules. We discuss how this mechanism of phage-host co-evolution impacts the tail specificity apparatus of *Acinetobacter* podoviruses.

Introduction

Bacteriophages (phages) are ubiquitous in nature, often outnumbering by tenfold the bacterial counts (Proctor *et al.*, 1988; Bergh *et al.*, 1989). These virions are considered a major driving force of bacterial evolution (Koskella and Brockhurst 2014), being known to modify competition among bacterial strains or species (Bohamann and Lenski, 2000; Joo *et al.*, 2006; Koskella *et al.*, 2012), maintain bacterial diversity (Buckling and Rainey, 2002; Rodriguez-Valera *et al.*, 2009), and mediate horizontal gene transfer among bacteria (Kidambi *et al.*, 1994; Canchaya *et al.*, 2003). Likewise, the arms-race between phages and bacteria has been shown to affect global nutrient cycling (Suttle, 2007) and climate (Fuhrman, 1999; Suttle, 2007), and the evolution of virulence in human pathogens (Brüssow *et al.*, 2004). There is a remarkable and dynamic genetic diversity of both phages and bacteria which results in different types of interactions (Pedulla *et al.*, 2003). A fundamental aspect of phage-host interaction is phage specificity, that is, the phage capacity to infect a specific bacterial host. Phage specificity is governed by the ability of the phage to adsorb to the bacterial cell wall, to inject the viral genome through the cell membrane, to express viral genes and replicate the genome in the host cell, and to release progeny virions after cell lysis (Kutter and

Sulakvelidze, 2004; Drulis-Kawa *et al.*, 2012; Henry and Debarbieux, 2012). Of these, phage adsorption is the crucial step for the onset of infection. The process of phage adsorption to a susceptible host cell is determined by the specific interaction between the phage receptor-binding protein (RBP) and a specific receptor on the surface of the host cell. Phage RBPs and their particular characteristics are diverse and include tail fibres, tail spikes and tail tips, with or without enzymatic activity (reviewed in (Rakhuba *et al.*, 2010; Chaturonga-kul and Ounjai, 2014)). The host-associated receptors used by phages for adsorption are extensive and range from peptide sequences to polysaccharide moieties (Bertozzi Silva *et al.*, 2016). In many cases, the host receptor used for reversible adsorption is distinct from that involved in irreversible binding (Baptista *et al.*, 2008; Vinga *et al.*, 2012; Bertozzi Silva *et al.*, 2016). The reversible adsorption is thought to occur to receptors more exposed and easier to access, to increase the probability of finding the cell receptor associated with irreversible binding (Chatterjee and Rothenberg, 2012). A phage loses the ability to effectively infect its host if the receptors become inaccessible, for example by the production of a capsule, commonly composed of poly-saccharides or proteins, that obstructs the access of phages to the surface of the host cell (Labrie *et al.*, 2010). However, some phages have developed long tail fibres to penetrate this layer and reach the internal receptor, and others have acquired the ability to use the capsule as an adsorption receptor and to degrade them through hydrolysis (Samson *et al.*, 2013; Pires *et al.*, 2016). The degradation of the layer is the reversible step of adsorption, which enables phage to penetrate the capsule and gain access to the secondary receptor on the outer membrane (Rakhuba *et al.*, 2010). A well-known example of a phage able to degrade the bacterial capsule is coliphage K1F which expresses an endosiali-dase that recognizes and degrades the K1 capsule of *Escherichia coli* (Scholl *et al.*, 2005). Most of the phages identified to have RBP recognizing exopolysaccharides are *Podoviridae* (Bertozzi Silva *et al.*, 2016), but little is known about the evolution of phages infecting encapsu-lated bacteria. To understand how these phages have evolved, we used a set of phages specific for bacteria of the *Acinetobacter calcoaceticus-Acinetobacter bauman-nii* (ACB) complex as a model system. The ACB complex forms a distinct phylogenetic lineage of the Gram-negative genus *Acinetobacter* (Touchon *et al.*, 2014) and comprises the closely related species *A. bau-mannii*, *A. calcoaceticus*, *Acinetobacter dijkshoorniae*, *Acinetobacter nosocomialis*, *Acinetobacter pitti*, and *Aci-netobacter seifertii* (Nemec *et al.*, 2011; 2015; Cosgaya *et al.*, 2016). While *A. calcoaceticus* is primarily a soil organism, the other species of the ACB complex, with

A. baumannii in particular, have been implicated in noso-comial infections worldwide (Antunes *et al.*, 2014) with rising antibiotic resistance rates (Ventola, 2015). The capsule surrounding the bacterial cell is one of the few known virulence determinants (Russo *et al.*, 2010). The capsule synthesis locus is found at the chromosomal K locus (KL), usually flanked by *fkpA* and *lldP* genes. This locus determines the capsule structure type (K type) by defining the oligosaccharide units (K units) formed. The K units formed at the cytoplasmic face of the inner mem-brane are translocated across the membrane by the *Wzx* flippase, and linked together by the *Wzy* polymer-ase to form the capsule (Whitfield, 2006; Kenyon and Hall, 2013). In *Acinetobacter* species, the capsule comes in many K types, reflecting the different sets of genes of the KL coding for the enzymes responsible for capsule synthesis, assembly, and export (Hu *et al.*, 2013; Kenyon and Hall, 2013; Kenyon *et al.*, 2014, 2015a,b,c). Typically, KL includes the export genes at one end, the genes for synthesis of common sugar pre-cursors at the other end, and a highly variable region in between that includes the remaining genes (e.g., genes coding for pseudaminic acid (*Psa*), legionaminic acid (*Lag*), 8-epilegionaminc acid and acinetaminic acid) (Kenyon and Hall, 2013; Kenyon *et al.*, 2014, 2015a,b,c; Shashkov *et al.*, 2015a,b). Compared with the 80 and 81 different capsular K antigens documented in *E. coli* and *K. pneumonia* species respectively (Whitfield and Roberts, 1999; Pan *et al.*, 2013), at least 106 capsular types exist in *A. baumannii* (Kenyon *et al.*, 2017). This vast and complex variety of capsular structures hampers the development of an efficient typing scheme currently inexistent for *Acinetobacter* species. This would, however, make a perfect model to study the host-specificity determinants of ACB phages harbouring depolymerases.

It is expectable that phages targeting ACB species will be able to recognize and degrade their capsule, as already demonstrated for phage ØAB6 (Lai *et al.*, 2016). Likewise, the composition of the capsule will certainly dictate the ability of the phage to infect the strains. Indeed, phages infecting *Acinetobacter* species tend to have a very narrow host range (Lin *et al.*, 2010), which may well be related to the variable composition of the bacterial capsule. However, so far, little is known about the evolutionary origin of phages specific to the ACB complex and the genetic infor-mation is very limited because of the scarce number of phage genome sequences available. In the present study, we have isolated and characterized 12 phages infecting the ACB complex. Genome comparison of 5 newly isolated phages and all *Acinetobacter* podoviruses deposited in Genbank provided detailed insights into the genetic varia-tion of the ACB complex-associated capsule-degrading podoviruses. We also correlated phage specificity to a
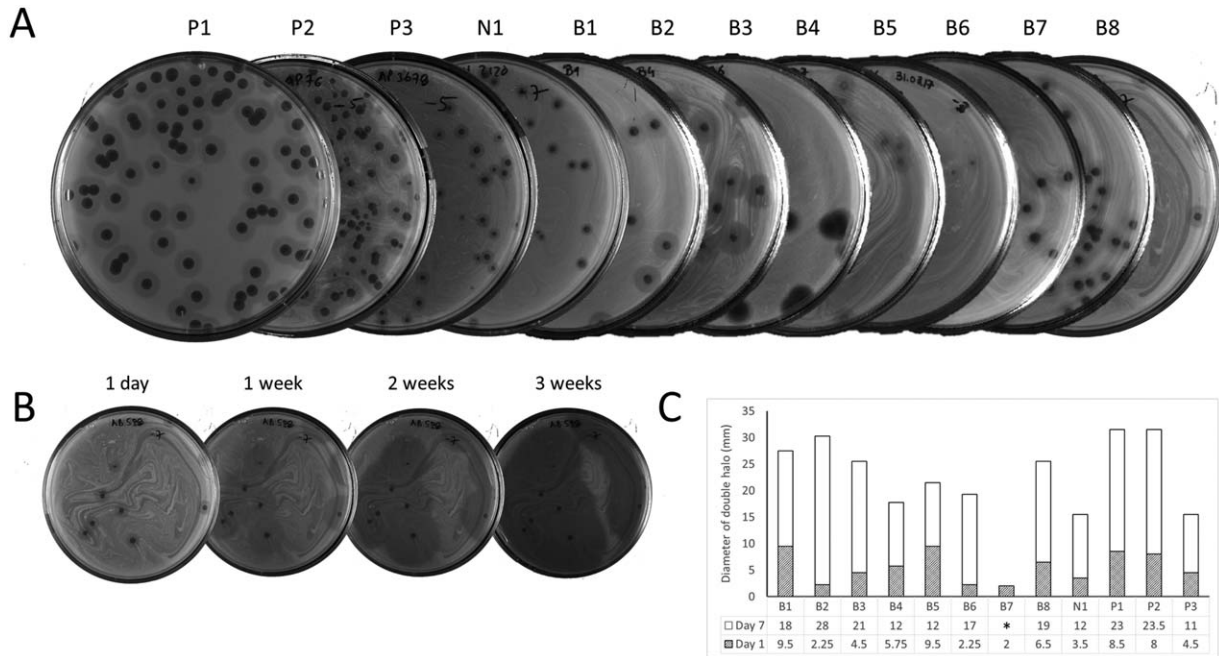
Fig. 1. Plaque characteristics of isolated *A. calcoaceticus-A. baumannii* complex-infecting phages. (A) Plaque morphologies of *A. baumannii*-infecting phages (B1, B2, B3, B4, B5, B6, B7 and B8), *A. pittii*-infecting phages (P1, P2 and P3) and *A. nosocomialis*-infecting phage (N1) on double layer TSA plates (0.6% (wt/vol) soft agar); (B) Example of the evolution of a phage plaque and surrounding halo during 3 weeks for B8; (C) Graphical representation of the halo increasing diameters for all isolated phages, from day 1 to day 7. *Size undetermined because bacterial growth masked halo.

pattern of recognition of the bacterial K type by each particular phage depolymerase.

Results

New ACB complex-infecting phages produce plaques with opaque halos and are podoviruses

A total of 12 phages were successfully isolated from different sewage samples collected over a period of 3 months, and revealed the presence of phage plaques surrounded by halo rings (Fig. 1A). These phages had, however, different halo sizes which increased over time (Fig. 1B and C). For instance, phage B2 halo diameter increased 25.75 mm in one week (halo of 28 mm), while phage B5 halo increased 9.50 mm (halo of 12 mm) in the same period. We further examined the phage and bacterial counts on equal surface size of the different zones: lysis, halo and bacterial area. Phage titre decreased from 1×10^6 PFU/ml to 2×10^5 PFU/ml and 0 PFU/ml counts respectively, whereas bacterial counts increased from 0 CFU/ml to 1×10^3 CFU/ml and 3×10^5 CFU/ml in the same areas.

TEM micrographs revealed that all phages belong to the order *Caudovirales* and are morphologically similar (Supporting Information Fig. S1). All viruses have short non-contractile tails ranging from 9 to 12 nm in length and 50 to 60 nm isometric heads, resembling *Podoviridae*

morphotype C1 phages, which include coliphage T7 (Ackermann, 1998).

All ACB complex podoviruses have distinct narrow host ranges but similar infective parameters

The phage lytic spectra were analysed against a panel of 49 well characterized strains of the ACB complex, collected at different time periods and geographical regions across the planet (Nemec *et al.*, 2015). We observed a narrow host range for all podoviruses (Supporting Information Table S1). Phages B4, B6 and P3 have an equal spectrum of infectivity, lysing one *A. baumannii* (NIPH 290) and four *A. pittii* (NIPH 519[T], NIPH 3678, NIPH 3870 and CEB-Ab) strains; phages P1 and B7 have an almost identical host range to the previous, with the exception of being unable to infect NIPH 519[T]; phage P2 infects two *A. pittii* strains (NIPH 519[T] and NIPH 76); phages B1, B5 and B8 infect two *A. baumannii* strains (NIPH 80 and NIPH 528); phage B3 infects one *A. baumannii* (NIPH 2061) and one *A. nosocomialis* (NIPH 2120) strain; and phages B2 and N1 infect only one strain, *A. baumannii* NIPH 70 and *A. nosocomialis* NIPH 2120 respectively. Generally, all phages plated efficiently in sensitive hosts, with only two cases of lysis from without (Supporting Information Table S1). We further observed that the opaque halo zone surrounding the

plaques was present in every infected strain, coupling phage sensitivity and halo formation.

To study the phage infective parameters, adsorption and one-step-growth experiments were conducted (Table 1). Phage adsorption rates to different *Acinetobacter* propagating hosts were similar ranging from 96.2% (phage P3) to 99.4% (phage P2), with the exception of phage B5 with a slightly lower value of 84.8% (Table 1). Phage adsorption to non-propagating hosts was also determined (Supporting Information Table S2). Adsorptions were in general similar ($P > 0.01$), with the exception of adsorption rates of phages B4, B6, P2 and P3 to *A. pittii* NIPH 519, with values significantly ($P < 0.01$) lower than those obtained for the remaining infected strains; and of phage B5 to *A. baumannii* NIPH 80, which were significantly ($P < 0.01$) higher than those obtained for the propagating host (*A. baumannii* NIPH 528). Conversely, one-step growth cycles demonstrated latent periods varying from 10 to 25 min, and low (6–9 PFUs/per infected cell for B1, B2, B4 and N1), medium (16–75 PFUs/per infected cell for B5, B6, B7, P1, P2 and P3) and high (117–200 PFUs/per infected cell for B3 and B8) burst sizes (Table 1).

Podovirus genomes present variations in the local pectate lyase domain

To study the genomic properties of the isolated ACB-infecting phages, we selected and sequenced five podoviruses (P1, P2, B1, B3 and B5) with different lytic spectrums. The general genomic characteristics are summarized in Table 1, with detailed annotation in Supporting Information Tables S3–S7. The genomes of P1, P2, B1, B3 and B5 have a length ranging from 40 598 to 41 608 bp, an average G + C content of 39.1–39.3%, which overlaps with the range of 38.6–39.3% found for the 31 ACB bacterial genomes included in this work. They encode 49–56 CDSs with high identities (> 85% average amino acid identity) to proteins of other *A. baumannii* podophages, such as phages Abp1 (NC_021316), phiAB1 (NC_028675), PD-AB9 (NC_028679), PD-6A3 (NC_028684), Fri1 (NC_028848), phiAB6 (NC_031086), AS11 (KY268296), AS12 (KY268295), WCHABP5 (KY888680), IME200 (NC_028987), SH-Ab 15519 (KY082667), Petty (NC_023570) and Acibel007 (NC_025457) (Chang *et al.*, 2011; Huang *et al.*, 2013; Mumm *et al.*, 2013; Merabishvili *et al.*, 2014; Lee *et al.*, 2017; Popova *et al.*, 2017).

Regarding genetic organization, all phages have defined DNA metabolism and replication, DNA packaging and lysis modules. Notably, whole-genome comparisons of the newly sequenced phages and all *Acinetobacter* podoviruses available in Genbank have shown an almost perfect genomic synteny and generally high homology (> 80%) (Fig. 2A and Supporting Information Table S8). These

Table 1. General features of the podoviruses infecting the *A. calcoaceticus-A. baumannii* complex.

Characteristic	B1	B2	B3	B4	B5	B6	B7	B8	P1	P2	P3	N1
Bacterial Species	*A. baumannii*	*A. baumannii*	*A. baumannii*	*A. baumannii*	*A. baumannii*	*A. baumannii*	*A. baumannii*	*A. baumannii*	*A. pittii*	*A. pittii*	*A. pittii*	*A. nosocomialis*
Lifestyle	Lytic	Lytic	Lytic	Lytic	Lytic	Lytic	Lytic	Lytic	Lytic	Lytic	Lytic	Lytic
Virus family	Podoviridae	Podoviridae	Podoviridae	Podoviridae	Podoviridae	Podoviridae	Podoviridae	Podoviridae	Podoviridae	Podoviridae	Podoviridae	Podoviridae
Capsid length, width (nm)	52 ± 1.9	50 ± 1.6	60 ± 2.5	50 ± 1.8	57 ± 2.2	52 ± 2.9	57 ± 2.2	48 ± 1.9	50 ± 1.4	52 ± 1.5	52 ± 1.4	50 ± 1.8
Tail length (nm)	12 + 1.4	12 ± 1.8	12 ± 0.8	15 ± 1.3	11 ± 1.5	11 ± 1.7	12 ± 1.5	11 ± 1.5	11 ± 1.2	10 ± 0.8	9 ± 1.3	12 ± 0.6
Latency period (min)	25	15	20	15	15	20	20	20	15	15	10	20
Burst size (PFU/cell)	8.06 ± 1.7	8.89 ± 1.9	116.7 ± 76.3	5.8 ± 1.18	25.0 ± 7.1	43.7 ± 7.1	55.5 ± 9.62	200.0 ± 0.0	75.4 ± 5.2	15.8 ± 3.8	26.7 ± 9.4	5.8 ± 1.2
Adsorption degree (%)a	97.9 ± 0.7	99.0 ± 0.6	98.1 ± 1.2	98.8 ± 0.6	84.8 ± 1.7	97.9 ± 1.3	98.3 ± 1.4	99.0 ± 0.4	98.9 ± 1.0	99.4 ± 0.3	96.2 ± 2.3	98.4 ± 0.2
Genome size (bp)	40,879	–	40.598	–	41,608	–	–	–	41,208	41,514	–	–
G+C content	39.1	–	39.3	–	39.3	–	–	–	39.2	39.3	–	–
CDS with function/ total CDS	24/51	–	24/49	–	22/56	–	–	–	21/49	22/54	–	–
N° of unique CDS	1	–	1	–	1	–	–	–	1	2	–	–

a. After 5 min.
The taxonomy, morphology and lytic data are given for all isolated phages. Genome features are also given for the five sequenced phages in this study (P1, P2, B1, B3 and B5).
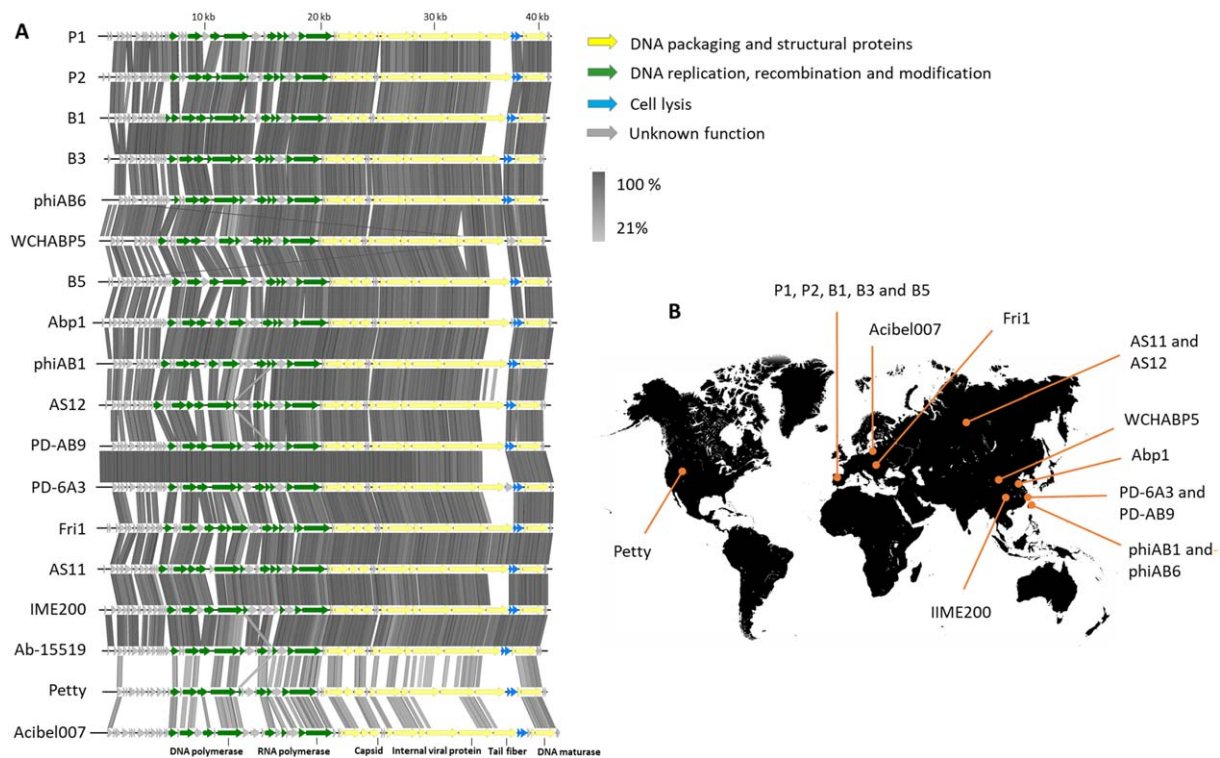
Fig. 2. Diversity of phages infecting the *A. calcoaceticus-A. baumannii* complex. (A) Multiple genome alignment; and (B) geographical distribution of all *Acinetobacter*-infecting podoviruses, namely, the newly sequenced P1 (MF033350), P2 (MF033351), B1 (MF033347), B3 (MF033348) and B5 (MF033349) and the previously sequenced *A. baumannii* phages Abp1 (NC_021316), phiAB1 (NC_028675), PD-AB9 (NC_028679), PD-6A3 (NC_028684), Fri1 (NC_028848), phiAB6 (NC_031086), AS11 (KY268296), AS12 (KY268295), WCHABP5 (KY888680), IME200 (NC_028987), SH-Ab 15519 (KY082667), Petty (NC_023570) and Acibel007 (NC_025457). The geographical position of SH-Ab 15519 is unknown. Genome map illustrates all putative CDSs drawn at scale, with colours grey, green, yellow and blue attributed according to their predicted function.

phages were isolated in different areas around the world (Asia, Europe and Africa) (Fig. 2B), so this high genomic similarity suggests a common phylogeny and close relatedness of these viruses.

Notably, a lack of homology was observed only for the gene coding for tail fibres (e.g., P1gp43, P2gp48, B1gp45, B3gp42 and B5gp47). The molecular structure of this encoded protein has an N-terminal phage_T7_tail domain (PF03906), corresponding to the main structural part of these proteins, and a C-terminal pectate_lyase_3 domain (PF12708), which is presumably the enzymatic part of the tail fibre with depolymerase activity. Generally, the N-terminal regions were highly conserved among all phages (BLASTP; *E*-value < 4 E -71; $> 80\%$ identity), while the C-terminal coding for the pectate lyase domain was highly diverse, with no significant homologous in the Genbank database. Cases of highly similar ($>$ 90% average amino acid identity) pectate lyase domains were detected between phages B3, phiAB6 and WCHABP5, between Fri1 and AS11, and with IME200 and SH-Ab-15519. Homology among AS12 and phiAB1 depolymerases was also detected only with a relatively low homology (53% average amino acid identity).

The recombinant pectate lyase displays depolymerase activity

We cloned the pectate lyase domain from the tail fibre gene of *A. pittii* phage P1 to investigate its function. The recombinantly produced protein was highly soluble (2.78 mg/ml) and active. When tested against all strains used in this study (Supporting Information Table S9), the enzyme followed the exact range of host spectrum activity (*A. baumannii* NIPH 290 and *A. pittii* ANC 3678, ANC 3870 and CEB-Ap) of its phage P1. The protein was able to produce opaque halos at concentrations between 0.1 and 1000 μg/ml (Fig. 3), and was equally active after 2-year storage at 4°C. The depolymerase nature of the P1 pectate lyase was confirmed by observing its activity towards extracted exopolysaccharides from the P1 host and other two non-infected strains. The $OD_{535\ nm}$ values of the extracted exopolysaccharides incubated with PBS were 0.33 ± 0.04 for host *A. pittii* CEB-Ap, 0.33 ± 0.04 for *A. baumannii* NIPH 2061 and 0.34 ± 0.04 for *A. baumannii* NIPH 201. When incubated with P1 depolymerase, the OD_{535nm} values were 0.91 ± 0.04 for *A. pittii* CEB-Ap, 0.32 ± 0.03 for *A. baumannii* NIPH 2061 and 0.32 ± 0.04
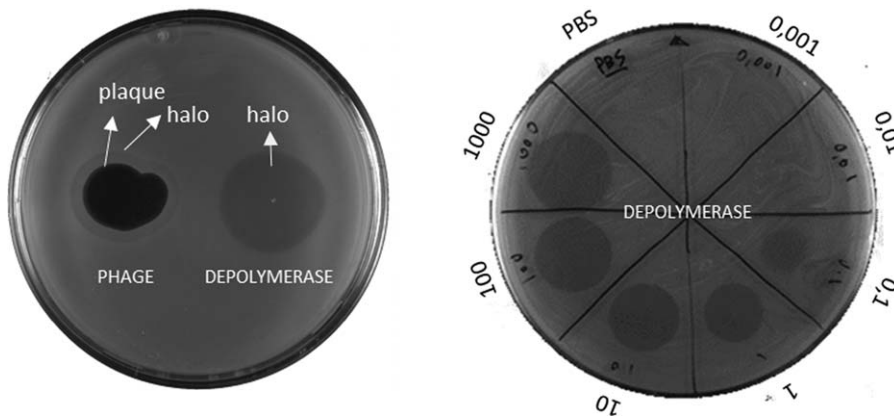
Fig. 3. Phage P1 depolymerase activity. (A) Spot-on-lawn test of phage P1 and its recombinant depolymerase; (B) spot test of 5 μl of serial dilutions of P1 recombinant depolymerase (0.0001–1000 mg/ml) on host strain. PBS buffer was used as a control.

for *A. baumannii* NIPH 201. The increase of the OD_{535} nm of the extracts incubated with P1 depolymerase, as a result of the presence of reducing sugars, indicates enzymatic degradation (Student's *t* test, $P < 0.01$), which was only detected on the exopolysaccharides extracted from the host strain *A. pittii* CEB-Ap.

Atomic force microscopy (AFM) analyses of whole-cell mount preparations were also used to assess the effect of P1 depolymerase on the *Acinetobacter* bacterial K types (Fig. 4). Generally, it was easier to see the presence of capsule on amplitude than in topography images. In Fig. 4A and B, fine details of the cell envelope, including the capsules were observed in the P1 host, as expected. In Fig. 4C and D, cells previously treated with P1 depolymerase had no identifiable capsules. Therefore, we conclude that pectate lyase had a depolymerase activity generating capsule-stripped cells.

Virion-associated exopolysaccharide depolymerases recognize host receptors

To understand if bacterial capsules acted as the primary phage receptor, adsorption assays were performed on P1 propagating and non-propagating host cells pretreated with P1 recombinant depolymerase to generate capsule-stripped bacterial cells. Results demonstrate that > 99% of P1 particles adsorbed when incubated with wild type P1 propagating host (*A. pittii* CEB-Ap), as expected. In opposite, only 39% of virions were detected with depolymerase-treated cells, suggesting they were unable to efficiently adsorb onto the bacterial surface. Identical results were observed for the other hosts: 94% versus 29% for untreated and depolymerase-treated *A. baumannii* NIPH 290, 94% versus 16% for untreated and depolymerase-treated *A. pittii* NIPH 3678, and 98% versus 11% for untreated and depolymerase-treated *A. pittii* NIPH 3870. No P1 particles were found adhered to both untreated and depolymerase-treated non-host *A. baumannii* NIPH 201, used as a negative control. We hypothesize that P1

depolymerase is interacting or degrading the bacterial capsules and the lower adsorption to stripped cells suggests that capsules are the primary receptor of phage P1.

De novo genome sequencing place CEB-Ap in the A. pittii species

The genome of host strain CEB-Ap of phage P1 was previously uncharacterized and we, therefore, sequenced its genome using Illumina HiSeq technology and performed a *de novo* genome assembly. The sequencing initially yielded 22.1 million read pairs of 50 bp length (for each single read). Since the genome of *Acinetobacter* species is around 4 Mb in size, this corresponded to a $> 250\times$ coverage. The assembly (GenBank accession no. NGAB00000000) yielded 108 contigs (> 200 bp) with a total size of 3.996 Mbp, GC-content of 38.71% and an n50 of 123 273 bp. Annotation by NCBI's automated pipeline detected 3908 genes including 115 pseudogenes, 26 tRNA genes, 3 rRNA genes and 4 other non-coding RNAs. The 16S and 23S genes are located on the same contig, which exhibited a 5–6-fold increased coverage, corresponding well to the presence of 6 paralogous ribosomal gene clusters as reported in the Ribosomal RNA database *rrnDB* (https://rrndb.umms.med.umich.edu/). Aligning the sequence of the 16S gene to the RDP database using the SeqMatch tool (https://rdp.cme.msu.edu/seqmatch) showed high sequence similarity (score 0.996–1.000) to strains of the species *A. calcoaceticus* and *A. pittii*. To obtain a more exact phylogenetic placement of CEB-Ap, its whole genome sequence was compared with those of the type strains of the ACB complex species using the average nucleotide identity based on BLAST (ANIb) and digital DNA–DNA hybridization (dDDH) parameters, calculated with the JSpecies (http://www.imedea.uib.es/jspecies) and GGDC 2.1 (http://ggdc.dsmz.de) programs respectively. The highest ANIb and dDDH values were found for *A. pittii* (97.5% and 89.9% respectively) followed by those for *A. dijkshoorniae* (93.1% and 51.8% respectively). In light of the recommended
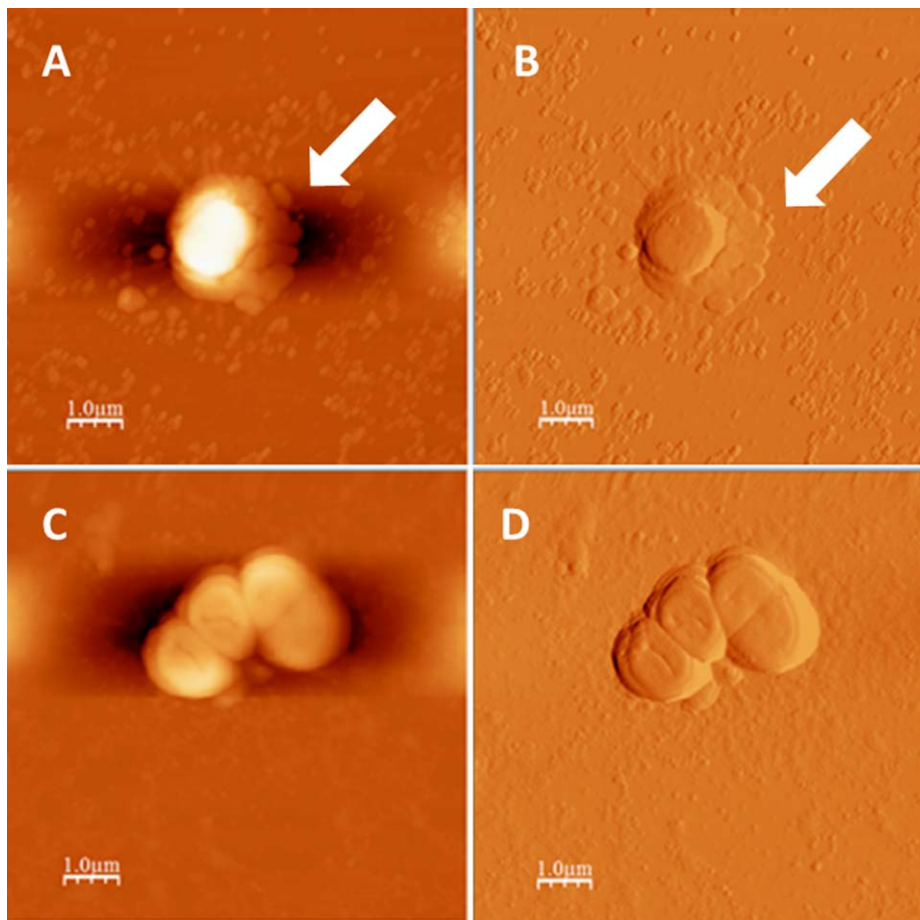
Fig. 4. AFM images of *A. pittii* strain CEB-Ap. The 2D-topography images (A and C) and amplitude images (B and D) for the wild-type (A, B) and P1 depolymerase-treated (C, D) CEB-Ap strain. Images were collected in Tapping mode™. The large arrows indicate the capsular material. Scale bars for each panel of 1 μm are shown. [Colour figure can be viewed at wileyonlinelibrary.com]

intraspecies ANIb and dDDH values [≥ 96% and ≥ 70% respectively (Meier-Kolthoff *et al.*, 2013; Rossello-Mora and Amann, 2015)], these results clearly place CEB-Ap in the *A. pittii* species.

*Phages harbouring depolymerases infect hosts with specific K types*

After observing the phage genomic differences at the depolymerase site and confirming the ability of these enzymes to interact with bacterial capsules, we investigated which K types were being degraded by comparing the KL types of all strains (Supporting Information Table S10).

The KL of strain CEB-Ap and 31 additional strains were located by detecting the flanking genes *wzc* and *pgm* and annotated following the Hall–Kenyon nomenclature (Kenyon and Hall, 2013). The genetic composition of the 31 KL is depicted in Fig. 5 and Supporting Information Fig. S2. Overall, each genome had a gene cluster between the *fkpA* and *lldP* genes resembling that found in *Acinetobacter venetianus* RAG-1 (Nakar and Gutnick, 2001), and generally with three putative transcripts with the second oriented in reverse direction relative to the others. The first

transcript contains conserved *wza*, *wzb* and *wzc* genes responsible for polysaccharide export. Transcript two is much longer and variable containing genes for repeat-unit synthesis (*wzx* and *wzy*) and at least one sugar pathway (e.g., UDP and CMP) among a varying collection of others. Transcript two generally also contained conserved genes located at the 5'-end, such as *galU*, *gne1*, *ugd* and *gpi*. Transcript three only contained the *pgm* gene in which all clusters ended. The specific functions of these genes have been extensively described elsewhere (Kenyon and Hall, 2013).

Only K types for *A. baumannii* strains have been previously assigned. However, linking the K type to phage host range, we observed that phages infect specific capsules (Fig. 5 and Supporting Information Fig. S2). Depolymerases of B3 and N1 phages recognize strains of the K2 type (*A. baumannii* NIPH 2061 and *A. nosocomialis* NIPH 2120, with equal KL). The K locus of these strains differs from all other by the presence of gene *kpsS1*, thought to encode the glycosyltransferase responsible for forming the final K2 linkage of pseudaminic acid to glucopyranose (Kenyon *et al.*, 2014); it is thus possible that the depolymerase is specific for and degrades this linkage.
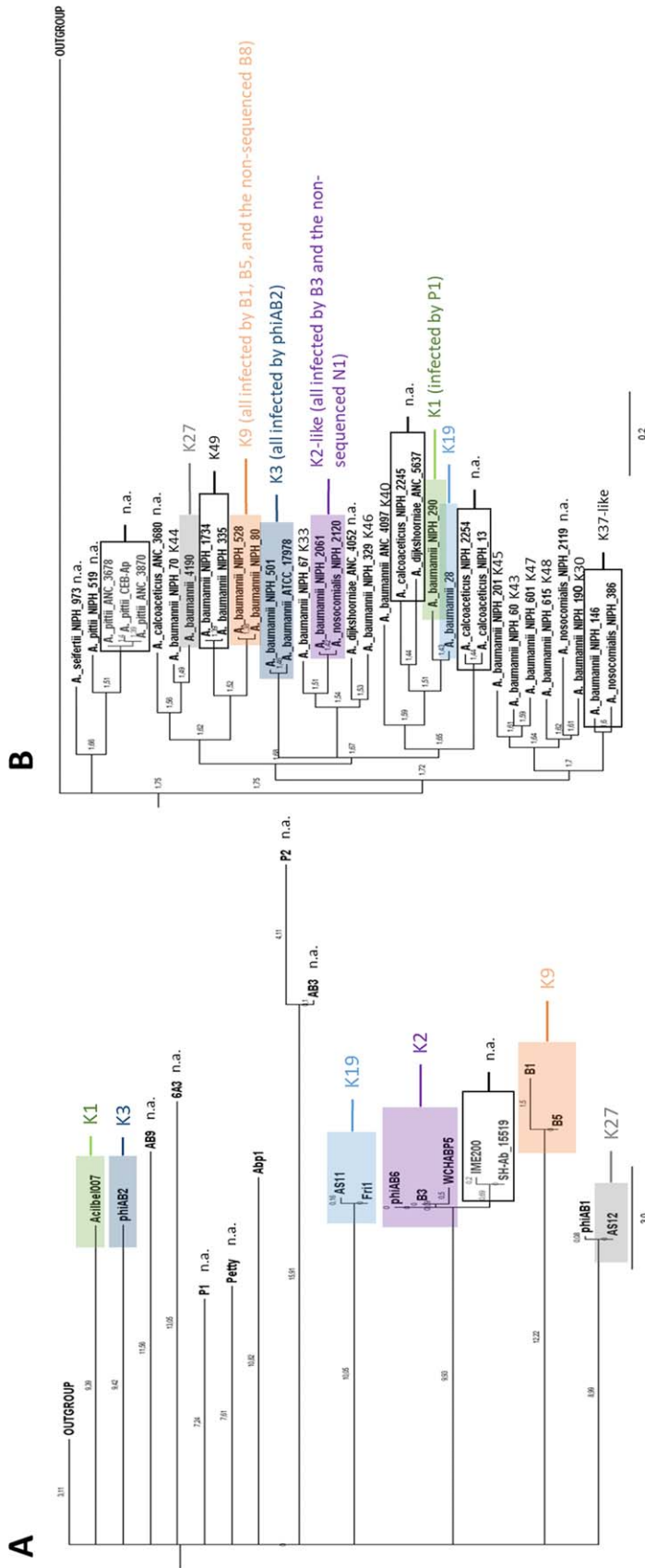
Fig. 5. Phylogenetic relationships. Phylogenetic analysis of (A) Phage depolymerase proteins and (B) K types of the *A. calcoaceticus-A. baumannii* complex (ACB) strains. The *Klebsiella* phage NTUH-K2044-K1-1 depolymerase (AB716666) and *Klebsiella* sp. 1015 DNA capsular synthesis operon (AB924551) were used as outgroups respectively. The trees were exported in Newick format and tree produced using FigTree. The coloured boxes define links between pectate lyase depolymerases and known K types which they recognize. Bank boxes indicate highly homologous depolymerase domains which recognize unknown K type, or highly homologous bacterial KL which synthesize an unknown K type. From the literature, the following additional sequences were retrieved from Genbank: *A. baumannii* ATCC 17978 (CP000521) of the K3 type which is host of phage phiAB2; *A. baumannii* 28 (KU215659.1) of the K19 type which is host of phages Fri1 and AS11; *A. baumannii* 4190 (KT266827) of the K27 type which is host of phage AS12. Both phages B6 and WCHABP5 infect strains with not-available genomes, but whose K2 types are reported elsewhere (Popova *et al.*, 2017). K type – capsule structure; K-like – at least one K type is known from a group of strains with highly similar K locus; n.a. – K not available. [Colour figure can be viewed at wileyonlinelibrary.com]

Depolymerases of phages B1, B5 and B8 are specific for K9 strains (*A. baumannii* NIPH 80 and NIPH 528). A comparison of the K locus of these strains with those of others shows the presence of genes *gnaB*, *gtr21* and *gtr22*, absent in all others. The product of *gnaB* converts N-acetyl-D-glucosaminuronic acid (GlcNAcA) into 2-acetamido-2-deoxy-D-galacturonic acid (GalNAcA) (Hu *et al.*, 2013), while the *gtr21* and *gtr22* glycosyltransferases may be involved in the formation of specific polysaccharide structures in the capsule; it is possible that the depolymerases of phages B1, B5 and B8 specifically bind to the GalNAcA of the bacterial capsule, or uses the specific linkages formed by these glycosyltransferases. For phage B2, the depolymerase targets only strain *A. baumannii* NIPH 70 displaying K44 type. Since this is the only strain used of this K type we cannot properly compare it to other K type strains to identify a possible specific target for the depolymerase. Still, this strain seems to be distinguishable from others solely by the glycosyltransferases used (*gtr56*, *gtr57* and *gtr58*), suggesting that the type of binding of the sugars in the capsule polysaccharides may be an important factor for depolymerase specificity. Depolymerases of phages B4, B6, B7, P1 and P3 seem to be less specific, infecting strains of different K types (K1 *A. baumannii* NIPH 290, undetermined K but highly similar KL of *A. pittii* NIPH 519, ANC 3678, ANC 3870 and CEB-Ap strains). These depolymerases may be recognizing a capsule epitope common to these strains; looking at Supporting Information Fig. S2, we observe that a common factor distinguishing these strains from all other is the absence of gene *gne*. This gene is thought to function in interconversion of UDP-N-acetylglucosamine (UDP-GlcNAc) and UDP-N-acetylgalactosamine (UDP-GalNAc), commonly resulting in the inclusion of GalNAc in the capsule structures (Hu *et al.*, 2013); this suggests that the depolymerases of phages B4, B6, B7, P1 and P3 have a preference for structures containing GlcNAc.

It is also interesting to observe from the phylogenetic tree of phage depolymerases in Fig. 5 that non-homologous depolymerases do not appear to have a common ancestor. It seems that a complete genetic drift in this region has occurred for the adaptation of the phages to new hosts.

Discussion

To adsorb and initiate infection, phages use receptor binding proteins to recognize specific host cell surface receptors. They are typically found at the phage tail fibres or protruding baseplate proteins and have been well characterized in coliphages and phages infecting lactic acid bacteria (Bertozzi Silva *et al.*, 2016). Concerning the nature and location of the host cell receptors recognized by phages, they vary greatly depending on the phage-host model (e.g., cell wall, pili, and flagella) (Guerrero-Ferreira *et al.*, 2011; Xia *et al.*, 2011; Shin *et al.*, 2012; Marti *et al.*, 2013). This is one of the reasons for the staggering diversity of phages on Earth and the vast evolutionary strategies adopted by them to infect a diverse group of bacterial hosts (Labrie *et al.*, 2010). In the particular case of exopolysaccharide slime or capsule surrounded bacteria, some phages have evolved the ability to produce virion-associated proteins with polysaccharide depolymerization activities (Pires *et al.*, 2016). Degradation of the bacterial capsules that act as the phage primary receptor enables phages to gain access to the host cell surface to bind irreversibly to a secondary receptor. While some works have studied the interaction of phage-borne depolymerases with *Bacillus anthracis*, *A. baumannii*, *Pseudomonas putida*, *Streptococcus equi* and *Erwinia amylovora* (Scorpio *et al.*, 2007; Cornelissen *et al.*, 2012; Singh *et al.*, 2014; Lai *et al.*, 2016), a more in depth research has been done only for phages infecting *Klebsiella pneumonia* and *E. coli* (Pelkonen *et al.*, 1992; Stummeyer *et al.*, 2006; Hsu *et al.*, 2013; Lin *et al.*, 2014; Majkowska-Skrobek *et al.*, 2016).

We have isolated and characterized phages infecting three (*A. baumannii*, *A. pittii*, and *A. nosocomialis*) of the six species of the ACB complex (Nemec *et al.*, 2015; Cosgaya *et al.*, 2016). All the isolated viruses had a narrow host range and the ability to produce opaque halos surrounding the phage plaques, similar to other reported phages infecting *A. baumannii* (Huang *et al.*, 2013; Merabishvili *et al.*, 2014; Lai *et al.*, 2016). These halo rings have been previously associated with depolymerase activities mostly in phages infecting *E. coli*, *P. putida* and *K. pneumoniae* and were found to be responsible for generating capsule-stripped cells (Pelkonen *et al.*, 1992; Cornelissen *et al.*, 2011; Cornelissen *et al.*, 2012; Hsu *et al.*, 2013). By analogy, the halos surrounding the newly isolated ACB phage plaques suggested areas of decapsulated *Acinetobacter* cells. As phage particles were always present in the halo zones, this also suggested the presence of putative virion-associated-depolymerases, and not soluble proteins expressed during phage infection. All halos were able to increase over time, like previously observed for instance for *P. putida* phages AF and Ø15 (Cornelissen *et al.*, 2011; 2012). Their expansion can be a result of free phages being able to degrade new capsules but unable to infect adjacent hosts, an overproduction of the tail fibre during the phage lytic cycle which was not assembled into the phage particle, or a consequence of a free depolymerase domain due to the synthesis of an alternative start codon.

TEM demonstrated that all phages were podoviruses, possibly linking the ability to produce depolymerase to this phage family. From a genomic perspective, all newly sequenced phages had close genomic resemblance to other *A. baumannii*-infecting podoviruses, for example,

Fri1, Abp1 and phiAB1. Interestingly, all ACB podoviruses (newly sequenced and all other sequences deposited in Genbank) shared a remarkable homology and collinearity, with the exception of a local and specific variation at the C-terminal region of the tail fibre genes, coding for a pectate lyase domain. This was unexpected given the high diversity of *Acinetobacter* strains and different time periods used to isolate these viruses. Furthermore, the vast geographical distribution of these viruses, spanning Asia, Europe and Africa, would make their genomic relatedness even more unlikely. The pectate lyase domain presumably encodes exopolysaccharide depolymerase activity and should be responsible for host specificity. These coding regions have been reported in other phage tail spikes to target and degrade specific K type, as observed for coliphage K5A (Thompson *et al.*, 2010) and Tsp2 of the *Klebsiella* KP36 phage (Majkowska-Skrobek *et al.*, 2016). A recent study has also shown that changing tail fibres of different *Acinetobacter* phages that encode pectate lyase domains results in a change of phage sensitivity to new hosts (Lai *et al.*, 2016). Nevertheless, all these reports have explored depolymerization activities of whole tail spike proteins, instead of using the specific depolymerase coding regions. Given the distinct narrow phage host ranges observed and the genomic difference mostly limited to the pectate lyase site, we intended to prove that these specific coding regions are the key components of the *Acinetobacter* podoviruses tail specificity apparatus.

The recombinantly expressed P1 pectase lyase domain exhibited depolymerase activity on bacterial lawns and towards extracted exopolysaccharides, and reduced the adsorption of phage P1 to host cells previously treated with the enzyme. The latter, together with the observation that the enzyme acts against the same strains infected by its parental phage (*A. baumannii* NIPH 290 and *A. pittii* ANC 3678, ANC 3870 and CEB-AP), suggests phage P1 uses the capsular polysaccharide as the primary receptor for phage adsorption and initiation of infection. Further studies are required to understand the precise role of the enzyme on the modification or cleavage of the capsule.

Linking our newly isolated phages together and all other podophages described in the literature with their infecting hosts (Fig. 5 and Supporting Information Fig. S2), we conclude that non-homologous depolymerase domains bind to distinct bacterial K types; the non-homologous depolymerases of P1, B1, B3, Fri1, AS12/phiAB1 and phiAB2 (from a partially sequenced phage deposited in Genbank GU979517) possibly recognize K1, K9, K2, K19 (Kenyon *et al.*, 2016), K27 (Shashkov *et al.*, 2015b) and K3 capsules (Lin *et al.*, 2010) respectively. The non-sequenced phage B2 recognizes capsule K44 and is, therefore, expected to encode another non-homologous depolymerase. Conversely, phages with homologous depolymerases infect bacteria with similar K types; for example,

depolymerases of B1 and B5 recognize K9, B3, phiAB6 and WCHAABP5 recognize K2 (Lee *et al.*, 2017; Popova *et al.*, 2017), Fri1 and AS11 recognize K19 (Kenyon *et al.*, 2016) and IME200 and SH-Ab-155519 recognize the same strain of unknown K type. It is interesting to note that these depolymerases are so specific that they are unable to recognize K types extremely close phylogenetically (see Fig. 5, for K2-like and K33, or K9 and K49 types). Interestingly, however, a few cases of promiscuous depolymerases were also detected; the depolymerases of phages B4, B6, P1 and P3 infect 3 strains with a highly similar KL but unknown K type (*A. pittii* ANC 3678, ANC 3870, CEB-Ap and NIPH 519), and one strain of K1 type (*A. baumannii* NIPH 290). It is possible that these two distinct K types share an epitope recognized by these depolymerases. Depolymerases with multicapsule activity have been described in *Klebsiella* phage K5-2 (Hsieh *et al.*, 2017). Although we could discover a few clues about the specific site of the capsule targeted by depolymerases (e.g., depolymerases of phages B3 and N1 may be targeting the K2-specific linkage of pseudaminic acid to glucopyranose, depolymerases of phages B1, B5 and B8 may be specifically binding to the GalNAcA of the KL9 capsule, and depolymerases of phages B4, B6, B7, P1 and P3 may have a preference for KL structures containing GlcNAc), the fully extent of recognition of *Acinetobacter* podophages encoding depolymerases will only be determined after sequencing more ACB podoviruses and after proper identification of additional capsule types for the non-*A. baumannii* host strains of phages IME200, SH-Ab-15519, Abp1, phiAB1, Petty and Acibel007. Generally, the results are congruent with the fact that phages infect specific or at least closely related K types. This is probably a result of the vast diversity of K structures acquired by ACB strains, which was counteracted by phages via the acquisition of distinct depolymerases, in a process of phage-host co-evolution.

In conclusion, this study illustrates the intricate interactions occurring between different and genetically identical podoviruses and species of the ACB complex. We proved that the pectate lyase domain of the phage tail fibres has depolymerization activities, and that depolymerase-capsule interaction is a key step for host recognition as capsule-stripped cells are not infected by the phage. Podoviruses infecting ACB species seemed to have evolved by the acquisition of specific pectate lyase coding regions, as a driving force for phage fitness.

Experimental procedures

Bacterial strains and culture conditions

Forty-nine strains of the ACB complex used for phage isolation and characterization in the present study are listed in Supporting Information Table S9. Except for one *A. pittii*

(CEB-Ap strain), all strains were from the collection of the Laboratory of Bacterial Genetics in Prague. They were selected to be diverse in both their origin and genotypic characteristics (as indicated by various multilocus sequence typing profiles). The selected strains belong to the six known species of the ACB complex, that is, *A. baumannii* ($n = 21$), *A. calcoaceticus* ($n = 7$), *A. dijkshoorniae* ($n = 5$), *A. nosocomialis* ($n = 5$), *A. pittii* ($n = 6$) and *A. seifertii* ($n = 5$). For 30 strains, draft genome-sequences were already available while the genome sequence of *A. pittii* CEB-Ap was determined in this study (Supporting Information Table S9). The strains were grown at 37°C in Tryptic Soy Broth (TSB) or on Tryptic Soy Agar (TSA, 1.2% (wt/vol) agar).

Phage isolation and propagation

Phages were isolated from samples collected from raw sewage wastewater treatment plant (Frossos, Braga, Portugal) by enrichment (Oliveira *et al.*, 2016). Briefly, raw inlet sewage was centrifuged, enriched with *Acinetobacter* strains listed in Supporting Information Table S9 and incubated overnight at 37°C. Supernatant was collected, filtered (0.22 μm), serially diluted in SM buffer (100 mM NaCl, 8 mM MgSO$_4$ 7H$_2$O, 50 mM Tris-HCl pH 7.5) and spotted on double layer agar plates of the isolation strains for the detection of isolated phages. Single plaques with distinct morphologies were picked using sterile toothpicks and spread with sterile paper strips into fresh bacterial lawns until a consistent plaque morphology was obtained. Purified phage plaques were then produced in solid media as previously described (Sambrook and Russel, 2001). Produced phages were collected by adding 3 ml of SM buffer to each plate and incubating overnight at 4°C with gentle rocking. The suspension was recovered, centrifuged at 9000 × *g* for 15 min, and the supernatant was filtered (0.22 μm). Phage titre was determined using the double layer agar assay as previously described (Sambrook and Russel, 2001). Briefly, serial dilutions of phages were platted with the host bacteria and TSB soft agar (0.6% (wt/vol) agar on TSA plates. After overnight incubation at 37°C, plaque forming units (PFUs) were counted and phage concentration (PFU/ml) was calculated.

Transmission electron microscopy

Transmission electron microscopy (TEM) measurements were performed to analyse phages and bacteria. Phage particles were sedimented (20 000 × *g*, 1 h, 4°C), washed twice and re-suspended in tap water, using a Beckman J2–21 (California) centrifuge. Phages were deposited on copper grids provided with carbon-coated Formvar films, stained with 2% (wt/vol) uranyl acetate (pH 4.0), and examined using a Jeol JEM 1400 transmission electron microscope.

Lytic spectra and efficiency of plating

The lytic spectra of the isolated phages was determined by spotting 10-fold serial dilutions of each phage on bacterial lawns of all strains of the ACB complex used in this study (Supporting Information Table S9). After overnight incubation at 37°C the effect of phages on bacterial lawns was visualized

and scored. The relative efficiency of plating (EOP) was calculated as the titre of the phage (PFU/ml) for each isolate divided by the titre obtained for the propagating host. Productive infection (lysis) was distinguished from lysis from without phenomena by the appearance of cell lysis only in the first dilution(s) for the latter case.

Adsorption assays

Phage solutions were added to mid-exponential growing *Acinetobacter* cultures at a multiplicity of infection of 0.001. After a 5 min incubation period at 37°C with shacking (120 rpm), 20 μl of phage samples were taken and immediately serially diluted in SM buffer. The remaining samples were centrifuged at 8000 × *g* for 1 min, and 20 μl of the supernatant were taken and also serially diluted in SM buffer. Dilutions of both samples were spotted on bacterial lawns of the host strain and plated in TSA to determine phage concentration. The degree of adsorption was calculated by measuring the relative amount of adsorbed or reversibly adsorbed phages in the supernatants in comparison with total phage titre.

One step growth curves

One step growth curves were performed to calculate the latent period and burst size, as described previously (Oliveira *et al.*, 2016). Mid-exponential growing *Acinetobacter* cultures (10 ml) were centrifuged (7000 × *g*, 5 min, 4°C) and re-suspended in 5 ml of TSB. Phages were added at a multiplicity of infection of 0.001 and allowed to adsorb 5 min. Cultures were centrifuged (7000 × *g*, 5 min, 4°C) and suspended in 10 ml. After 5, 10, 15, 20, 25, 30, 40, 50 and 60 min, aliquots from each dilution were collected, serially diluted and plated. After overnight incubation at 37°C, phage particles were quantified.

Phage genome sequencing

Acinetobacter phage genomic DNAs were extracted by standard methods with phenol-chloroform-isoamyl alcohol as described elsewhere (Sambrook and Russel, 2001). DNA was sequenced using Illumina HiSeq platform (Illumina, San Diego, CA) with individual libraries of two non-homologous phages pooled together in equal amounts. Libraries were constructed using the KAPA DNA Library preparation kit for Illumina, with KAPA HiFi preparation protocol, and sequenced using 100 bp in paired-end mode. The quality of the produced data was determined by Phred quality score at each cycle. Reads were demultiplexed and *de novo* assembled into a single contig with average coverage above 100× using CLC Bio Genomics Workbench v7.0 (Aarhus, Denmark) and manually inspected.

Phage genome annotation and comparative genomics

Phage genomes were annotated using MyRAST algorithm (Aziz *et al.*, 2008). Putative functions were assigned to coding sequences (CDSs) by BLASTP (Altschul *et al.*, 1990) with tRNAs being predicted with tRNAscan-SE (Schattner *et al.*, 2005) and ARAGORN (Laslett and Canback, 2004). HHPRED (Soding *et al.*, 2005) was used to detect protein homology and

structure prediction. Protein transmembrane domains were found using Phobius (Kall *et al.*, 2004), TMHMM (Kall and Sonnhammer, 2002), HMMTOP (Tusnady and Simon, 2001) and N-terminal signal peptides with SignalP 3.0 (Bendtsen *et al.*, 2004). Transcriptional factors were determined by MEME (Bailey *et al.*, 2009) and ARNold (Naville *et al.*, 2011) for promoter and rho-independent terminators respectively. For comparative studies, genomics comparisons were made using BLASTN and EMBOSS stretcher (Rice *et al.*, 2000), while CoreGenes (Zafar *et al.*, 2002) and Easyfig (Sullivan *et al.*, 2011) were used to assess and visualize the proteome conservation.

Pectate lyase cloning, expression and purification

The pectate lyase domain of phage P1 located at the tail spike (genetic region 35 273 bp to 37 522 bp) was cloned into pTSL vector using primers (forward, CCAGGGCAGCGGATCC AATCCAAATTTAGATATGAGTGGATGG, reverse GTGCGG CCGCAAGCTTATGTAGCTTGTACGTTCCCTG, with restriction sites for BamHI and XhoI). Protein had N-terminal *E. coli* SlyD protein with $6 \times$ His-tag as a leader. The pTSL vector containing the SlyD protein was previously constructed (Taylor *et al.*, 2016). Hybrid protein expression was controlled by T7 promoter. The expression was performed at 16°C with vigorous shaking overnight. Cells were pelleted at $8000 \times g$, re-suspended in lysis buffer (50 mM Tris-HCl pH 8.0, 300 mM NaCl), and disrupted by sonication at 4–16°C (8–10 cycles with 30 s pulse and 30 s pause). The insoluble fraction was removed by centrifugation at $9000 \times g$ for 30 min at 4°C. The clarified cell lysate was loaded onto a 5-ml GE HisTrap FF Ni-charged column, and the protein was eluted with imidazole-containing buffer (50 mM Tris-HCl pH 8.0, 300 mM NaCl, 200 mM imidazole) using a step gradient. Fractions containing the protein were pooled and TEV protease added to give a protease:protein ratio of 1:100 (wt/wt). This mixture was dialysed into 10 mM Tris-HCl pH 8.0 by overnight incubation at 20°C resulting in cleavage of the His–SlyD expression tag. The digested protein was filtered and purified by ion-exchange chromatography using a MonoQ 10/100GL column and 0–1 M NaCl gradient in 20 mM Tris–HCl pH 8.0. Fractions containing the depolymerase were pooled and loaded onto a Superdex 75 HiLoad 16/60 size-exclusion column equilibrated with 10 mM PBS pH 7.0 and 150 mM NaCl.

Depolymerase activity

The recombinant P1 enzyme containing the pectate lyase domain was tested on several strains to evaluate its activity spectrum using the spot-on-lawn method. Mid-exponential growing cultures (100 μl) were plated with TSB soft agar to form lawns and a 10 μl enzyme drop was spotted in the middle. The occurrence of halo zones after 6 h of incubation at 37°C was indicative of sensitive strains. Different enzyme concentrations (0.001–1000 μg/ml) were used to evaluate the range of activity. PBS buffer was used as a control.

The activity of the P1 depolymerase was also tested against *A. pittii* strains CEB-P1 (P1 host) and NIPH 290 (P2 host) and *A. baumannii* strains NIPH 528 (B1 and B5 hosts) and NIPH 2061 (B3 host exopolysaccharides. The method applied has

been previously described (MIGL, 2012; Lee *et al.*, 2017). Briefly, CEB-P1 exopolysaccharides were extracted from 5-day-old cultures plates at 37°C, by adding 2.5 ml of 0.9% (wt/vol) NaCl per plate and by harvesting the cells. The mixture was incubated with 5% (vol/vol) phenol for 6 h, pelleted (10 000 $\times$ *g*, 10 min) and the surface polysaccharides precipitated with 5 volumes of 95% ethanol at −20°C overnight. The precipitate was spun down (6000 $\times$ *g* for 10 min), suspended in distilled water and treated with DNase (20 μg/ml) and RNase (40 μg/ml) for 1 h before being lyophilized. The enzymatic activity of P1 depolymerase was assessed by quantification of the reducing ends produced when reacting with 3,5-dinitrosalicylic acid (DNS). The lyophilized polysaccharides were dissolved in 20 mM HEPES/MES/sodium acetate (pH 5) and incubated with 5 mg/ml of the P1 pectate lyase recombinant enzyme or with PBS (control) at 37°C for 2 h. The reaction was stopped by heat inactivation (100°C for 15 min) and spun (8000 $\times$ g for 2 min) to remove denatured enzyme. Afterwards, 100 μl of the DNS reagent (10 mg/ml) was added to an equal volume of each reaction, heated to 100°C for 5 min and the absorbance measured at 535 nm.

Atomic force microscopy

AFM measurements were made to study the depolymerase effect on the bacterial capsules. *A. pitti* (CEB-Ap) overnight cultures were diluted in PBS to prepare final bacterial suspensions containing 10^8 CFU/ml. Bacterial suspensions were incubated with PBS (control sample) or with P1 depolymerase at 0.1 μg/ml final concentration (test sample) for 2 h. After incubation, 200 μl of each suspension were adsorbed in to a fresh cleaved mica, rinsed with Milli-Q water and air dried. AFM images were obtained with a PicoPlus5500 scanning probe microscope interfaced with a PicoScan controller (Keysight Technologies) using the PicoView 1.20 software (Keysight Technologies), coupled to an Inverted Optical Microscope (Observer Z1, Zeiss, Germany), to precisely choose the bacteria to be observed. Each sample was imaged with a 100×100 μm^2 piezoelectric scanner. All measurements were performed in Tapping^{TM} mode at room temperature using bar-shaped cantilever silicon tips (AppNano) with a spring constant of 25–75 N/m. Scan speed was set at 0.7 Hz with 512 lines. The scan angle was 0.0 ^{0}.

Identification of the phage receptor

To identify the bacterial capsule as the primary phage receptor, we studied the ability of phage P1 to adsorb to decapsulated cells. Mid-exponential growing cells of CEB-Ap (2 ml), the host of phage P1, were suspended to a density of 10^8 CFU/ml and incubated with an equal volume of the recombinant P1 pectate lyase enzyme (100 μg/ml, to destroy the capsule polysaccharide) or PBS (negative control). After 2 h at 37°C, cells were washed twice with TSB, and phage P1 added at a MOI of 0.001 and allowed to adsorb for 5 min. An identical procedure was performed for all non-host strains infected by phage P1 (*A. baumannii* NIPH 290, and *A. pittii* NIPH 519, ANC 3678 and ANC 3870), as well as for a non-infected strain used as negative control (*A. baumannii* NIPH 201). Adsorption was quantified as described above. The

difference in titration of enzyme-treated cells compared to the control experiment allowed us to evaluate the capacity of the phage to adsorb to decapsulated cells.

De novo *genome sequencing of strain CEB-Ap*

Genomic DNA of strain CEB-Ap was sequenced at the NGS core facility of the Karlsruhe Institute of Technology (KIT), Institute of Toxicology and Genetics (Karlsruhe, Germany). DNA sequencing libraries were produced from 1 μg of genomic DNA, following the recommendations of the TruSeq DNA protocol (Illumina). The DNA was sheared by sonication using a Covaris S2 instrument. Sizes and concentrations of DNA sequencing libraries were determined on a Bioanalyzer 2100 (DNA1000 chips, Agilent). Paired-end sequencing (2×50 bp) was performed on one lane on a Hiseq1500 (Illumina) platform using TruSeq PE Cluster KIT v3 – cBot – HS and TruSeq SBS KIT v3 – HS. Cluster detection and base calling were performed using RTA v1.13 and quality of reads assessed with CASAVA v1.8.1 (Illumina). The sequencing resulted in 22 million pairs of 50 nt long reads for each sample, with a mean Phred quality score > 35. The read data were clipped to remove low quality and adapter sequences using the fastq-mcf function of the ea-utils software (Aronesty, 2011; 2013) and assembled with the IDBA software (Peng *et al.*, 2012) using idba_hybrid with the complete genome of *A. pittii* PHEA-2 (GenBank accession no. NC_016603.1) as a reference. After the assembled genome was found to be more similar to *A. pittii*, the reads were assembled again with idba_hybrid using the genomic sequence of *A. pittii* NIPH 519^T (also known as CIP 70.29^T, GenBank accession no. NZ_KB849797.1), which did yield a nearly identical result. Scaffolds with less than 200 bp length were removed and the remaining scaffolds were aligned to the *A. pittii* CIP 70.29^T genomic sequence and re-ordered accordingly using Mauve (Trimble *et al.*, 2012). The final assembly was uploaded to NCBI GenBank with the accession number NGAB00000000 and associated with BioProject PRJNA386447. The genome was automatically annotated using the NCBI Prokaryotic Genome Annotation Pipeline (PGAP).

Identification of the Acinetobacter *spp. capsular synthesis loci (KL)*

The genomic region harbouring the CPS cluster genes was identified and annotated in *A. pittii* CEB-Ap and 31 previously sequenced strains of the ACB complex. For the initial localization, the genomic sequences were aligned by BLASTX against the conserved capsular proteins Wzc and Pgm, which represent the outer margins of the cluster. The individual genomic sequences of the strains' clusters were retrieved with the script seqs_subgroup_extr_016.py by Alexander Kozik (downloaded from github: https://github.com/alex-kozik/atgc-tools) using a range from 500 bp upstream of the *wzc* gene and 500 bp downstream of the *pgm* gene. When necessary, the cluster sequences were reverse complemented to obtain a parallel orientation with *wzc* on the left side. The gene content of each cluster was determined by detecting open reading frames with GeneMark and annotated using Blast according to a system proposed earlier [32]. Capsular polysaccharide

clusters of *A. baumannii* were designated according to references (Kenyon and Hall, 2013; Arbatsky *et al.*, 2015; Shashkov *et al.*, 2015a,b; 2016a,b; Arbatsky *et al.*, 2016). Possible transposons were determined using HHpred (Alva *et al.*, 2016).

Phylogenetic analysis

Two independent phylogenetic trees were constructed, one using the depolymerase pectate lyase domain sequences of the phages and other using the concatenated sequences of the K locus of ACB strains used in this study. Alignments of amino acid sequences were generated in Geneious (Kearse *et al.*, 2012) using MUSCLE (Edgar, 2004) with default settings. The phylogenetic trees were constructed using the Tamura-Nei genetic distance model with 100 boostrap. The trees were rooted using *Klebsiella* phage NTUH-K2044-K1-1 depolymerase (AB716666) and *Klebsiella* sp. 1015 DNA capsular synthesis operon (AB924551) as outgroups respectively.

Statistical analysis

Mean and standard deviations were determined for at least three independent experiments and results were presented as mean $\pm$ standard deviation. For extracellular polysaccharide experiments, adsorption assays and depolymerase assays, Student's t-test with a confidence level of 99% was used to show statistical difference between control and test conditions.

K locus nomenclature

In this study, we used standardized nomenclature previously proposed to describe the capsule synthesis locus of *A. baumannii* (Kenyon and Hall, 2013). Each distinct capsule synthesis locus was designated as KL (K locus) with a unique number. The K type reference K-loci were assigned the same number as the corresponding K type, for example, K1 is encoded by the KL1 locus.

Nucleotide sequence accession numbers

The complete genome sequences of phages P1, P2, B1, B3 and B5 have been deposited in GenBank under accession numbers MF033350, MF033351, MF033347, MF033348 and MF033349 respectively. The genome assembly and short read data were submitted to GenBank and the NCBI Sequence Read Archive (SRA) and are accessible via the Bio-Project accession PRJNA386447. The assembled and annotated genome of strain CEB-Ap was assigned the accession number NGAB00000000.

References

Ackermann, H.W. (1998) Tailed bacteriophages: the order *Caudovirales*. *Adv Virus Res* **51:** 135–201.

Altschul, S.F., Gish, W., Miller, W., Myers, E.W., and Lipman, D.J. (1990) Basic local alignment search tool. *J Mol Biol* **215:** 403–410.

Alva, V., Nam, S.Z., Soding, J., and Lupas, A.N. (2016) The MPI bioinformatics Toolkit as an integrative platform for advanced protein sequence and structure analysis. *Nucleic Acids Res* **44:** W410–W415.

Antunes, L., Visca, P., and Towner, K. (2014) *Acinetobacter baumannii*: evolution of a global pathogen. *Pathog Dis* **71:** 292–301.

Arbatsky, N.P., Shneider, M.M., Kenyon, J.J., Shashkov, A.S., Popova, A.V., and Miroshnikov, K.A. (2015) Structure of the neutral capsular polysaccharide of *Acinetobacter baumannii* NIPH146 that carries the KL37 capsule gene cluster. *Carbohydr Res* **413:** 12–15.

Arbatsky, N.P., Shneider, M.M., Shashkov, A.S., Popova, A.V., Miroshnikov, K.A., Volozhantsev, N.V., and Knirel, Y.A. (2016) Structure of the N-acetylpseudaminic acid-containing capsular polysaccharide of *Acinetobacter baumannii* NIPH67. *Russ Chem Bull* **65:** 588–591.

Aronesty, E. (2011). ea-utils: Command-line tools for processing biological sequencing data. URL http://code.google.com/p/ea-utils

Aronesty, E. (2013) Comparison of sequencing utility programs. *Open Bioinf J* **7:** 1–8.

Aziz, R.K., Bartels, D., Best, A.A., DeJongh, M., Disz, T., Edwards, R.A., *et al.* (2008) The RAST server: rapid annotations using subsystems technology. *BMC Genomics* **9:** 75.

Bailey, T.L., Boden, M., Buske, F.A., Frith, M., Grant, C.E., Clementi, L., *et al.* (2009) MEME SUITE: tools for motif discovery and searching. *Nucleic Acids Res* **37:** W202–W208.

Baptista, C., Santos, M.A., and São-José, C. (2008) Phage SPP1 reversible adsorption to Bacillus subtilis cell wall teichoic acids accelerates virus recognition of membrane receptor YueB. *J Bacteriol* **190:** 4989–4996.

Bendtsen, J.D., Nielsen, H., von Heijne, G., and Brunak, S. (2004) Improved prediction of signal peptides: SignalP 3.0. *J Mol Biol* **340:** 783–795.

Bergh, O., Borsheim, K.Y., Bratbak, G., and Heldal, M. (1989) High abundance of viruses found in aquatic environments. *Nature* **340:** 467–468.

Bertozzi Silva, J., Storms, Z., and Sauvageau, D. (2016) Host receptors for bacteriophage adsorption. *FEMS Microbiol Lett* **363:** fnw002.

Bohamann, B., and Lenski, R. (2000) The relative importance of competition and predation varies with productivity in a model community. *Am Nat* **156:** 329–340.

Brüssow, H., Canchaya, C., and Hardt, W.-D. (2004) Phages and the evolution of bacterial pathogens: from genomic rearrangements to lysogenic conversion. *Microbiol Mol Biol Rev* **68:** 560–602.

Buckling, A., and Rainey, P.B. (2002) The role of parasites in sympatric and allopatric host diversification. *Nature* **420:** 496–499.

Canchaya, C., Fournous, G., Chibani-Chennoufi, S., Dillmann, M.-L., and Brüssow, H. (2003) Phage as agents of lateral gene transfer. *Curr Opin Microbiol* **6:** 417–424.

Chang, K.C., Lin, N.T., Hu, A., Lin, Y.S., Chen, L.K., and Lai, M.J. (2011) Genomic analysis of bacteriophage varphiAB1, a varphiKMV-like virus infecting multidrug-resistant *Acinetobacter baumannii*. *Genomics* **97:** 249–255.

Chatterjee, S., and Rothenberg, E. (2012) Interaction of Bacteriophage λ with Its E. coli Receptor, LamB. *Viruses* **4:** 3162–3178.

Chaturongakul, S., and Ounjai, P. (2014) Phage–host interplay: examples from tailed phages and Gram-negative bacterial pathogens. *Front Microbiol* **5:** 442.

Cornelissen, A., Ceyssens, P.J., T'syen, J., Van Praet, H., Noben, J.P., Shaburova, O.V., *et al.* (2011) The T7-related *Pseudomonas putida* phage phi15 displays virion-associated biofilm degradation properties. *PLoS One* **6:** e18597.

Cornelissen, A., Ceyssens, P.J., Krylov, V.N., Noben, J.P., Volckaert, G., and Lavigne, R. (2012) Identification of EPS-degrading activity within the tail spikes of the novel *Pseudomonas putida* phage AF. *Virology* **434:** 251–256.

Cosgaya, C., Mari-Almirall, M., Van Assche, A., Fernandez-Orth, D., Mosqueda, N., Telli, M., *et al.* (2016) *Acinetobacter dijkshoorniae* sp. nov., a member of the *Acinetobacter calcoaceticus-Acinetobacter baumannii* complex mainly recovered from clinical samples in different countries. *Int J Syst Evol Microbiol* **66:** 4105–4111.

Drulis-Kawa, Z., Majkowska-Skrobek, G., Maciejewska, B., Delattre, A.-S., and Lavigne, R. (2012) Learning from bacteriophages - advantages and limitations of phage and phage-encoded protein applications. *Curr Protein Peptide Sci* **13:** 699–722.

Edgar, R.C. (2004) MUSCLE: multiple sequence alignment with high accuracy and high throughput. *Nucleic Acids Res* **32:** 1792–1797.

Fuhrman, J.A. (1999) Marine viruses and their biogeochemical and ecological effects. *Nature* **399:** 541–548.

Guerrero-Ferreira, R.C., Viollier, P.H., Ely, B., Poindexter, J.S., Georgieva, M., Jensen, G.J., and Wright, E.R. (2011) Alternative mechanism for bacteriophage adsorption to the motile bacterium *Caulobacter crescentus*. *Proc Natl Acad Sci USA* **108:** 9963–9968.

Henry, M., and Debarbieux, L. (2012) Tools from viruses: Bacteriophage successes and beyond. *Virology* **434:** 151–161.

Hsieh, P.F., Lin, H.H., Lin, T.L., Chen, Y.Y., and Wang, J.T. (2017) Two T7-like bacteriophages, K5-2 and K5-4, each encodes two capsule depolymerases: isolation and functional characterization. *Sci Rep* **7:** 4624.

Hsu, C.-R., Lin, T.-L., Pan, Y.-J., Hsieh, P.-F., Wang, J.-T., and Lin, B. (2013) Isolation of a bacteriophage specific for a new capsular type of *Klebsiella pneumoniae* and characterization of its polysaccharide depolymerase. *PLoS One* **8:** e70092.

Hu, D., Liu, B., Dijkshoorn, L., Wang, L., Reeves, P.R., and Nübel, U. (2013) Diversity in the major polysaccharide antigen of *Acinetobacter baumannii* assessed by DNA sequencing, and development of a molecular serotyping scheme. *PLoS One* **8:** e70329.

Huang, G., Le, S., Peng, Y., Zhao, Y., Yin, S., Zhang, L., *et al.* (2013) Characterization and genome sequencing of phage Abp1, a new phiKMV-like virus infecting multidrug-resistant *Acinetobacter baumannii. Curr Microbiol* **66:** 535–543.

Joo, J., Gunny, M., Cases, M., Hudson, P., Albert, R., and Harvill, E. (2006) Bacteriophage-mediated competition in Bordetella bacteria. *Proc R Soc B: Biol Sci* **273:** 1843–1848.

Kall, L., and Sonnhammer, E.L. (2002) Reliability of transmembrane predictions in whole-genome data. *FEBS Lett* **532:** 415–418.

Kall, L., Krogh, A., and Sonnhammer, E.L. (2004) A combined transmembrane topology and signal peptide prediction method. *J Mol Biol* **338:** 1027–1036.

Kearse, M., Moir, R., Wilson, A., Stones-Havas, S., Cheung, M., Sturrock, S., *et al.* (2012) Geneious Basic: an integrated and extendable desktop software platform for the organization and analysis of sequence data. *Bioinformatics* **28:** 1647–1649.

Kenyon, J.J., and Hall, R.M. (2013) Variation in the complex carbohydrate biosynthesis loci of *Acinetobacter baumannii* genomes. *PLoS One* **8:** e62160.

Kenyon, J.J., Marzaioli, A.M., Hall, R.M., and De Castro, C. (2014) Structure of the K2 capsule associated with the KL2 gene cluster of *Acinetobacter baumannii. Glycobiology* **24:** 554–563.

Kenyon, J.J., Marzaioli, A.M., De Castro, C., and Hall, R.M. (2015a) 5,7-di-N-acetyl-acinetaminic acid: A novel non-2-ulosonic acid found in the capsule of an *Acinetobacter baumannii* isolate. *Glycobiology* **25:** 644–654.

Kenyon, J.J., Marzaioli, A.M., Hall, R.M., and De Castro, C. (2015b) Structure of the K6 capsular polysaccharide from *Acinetobacter baumannii* isolate RBH4. *Carbohydr Res* **409:** 30–35.

Kenyon, J.J., Marzaioli, A.M., Hall, R.M., and De Castro, C. (2015c) Structure of the K12 capsule containing 5,7-di-N-acetylacinetaminic acid from *Acinetobacter baumannii* isolate D36. *Glycobiology* **25:** 881–887.

Kenyon, J.J., Shneider, M.M., Senchenkova, S.N., Shashkov, A.S., Siniagina, M.N., Malanin, S.Y., *et al.* (2016) K19 capsular polysaccharide of *Acinetobacter baumannii* is produced via a Wzy polymerase encoded in a small genomic island rather than the KL19 capsule gene cluster. *Microbiology* **162:** 1479–1489.

Kenyon, J.J., Shashkov, A.S., Senchenkova, S.N., Shneider, M.M., Liu, B., Popova, A.V., *et al.* (2017) *Acinetobacter baumannii* K11 and K83 capsular polysaccharides have the same 6-deoxy-l-talose-containing pentasaccharide K units but different linkages between the K units. *Int J Biol Macromol* **103:** 648–655.

Kidambi, S.P., Ripp, S., and Miller, R.V. (1994) Evidence for phage-mediated gene transfer among Pseudomonas aeruginosa strains on the phylloplane. *Appl Environ Microbiol* **60:** 496–500.

Koskella, B., and Brockhurst, M.A. (2014) Bacteria–phage coevolution as a driver of ecological and evolutionary processes in microbial communities. *FEMS Microbiol Rev* **38:** 916–931.

Koskella, B., Lin, D.M., Buckling, A., and Thompson, J.N. (2012) The costs of evolving resistance in heterogeneous parasite environments. *Proc R Soc B: Biol Sci* **279:** 1896–1903.

Kutter, E., and Sulakvelidze, A. (2004). *Bacteriophages: Biology and Applications*. Boca Raton, FL: CRC Press.

Labrie, S.J., Samson, J.E., and Moineau, S. (2010) Bacteriophage resistance mechanisms. *Nat Rev Microbiol* **8:** 317–327.

Lai, M.J., Chang, K.-C., Huang, S.-W., Luo, C.-H., Chiou, P.-Y., Wu, C.-C., and Lin, N.-T. (2016) The tail associated protein of *Acinetobacter baumannii* phage ΦAB6 is the host specificity determinant possessing exopolysaccharide depolymerase activity. *PLoS One* **11:** e0153361.

Laslett, D., and Canback, B. (2004) ARAGORN, a program to detect tRNA genes and tmRNA genes in nucleotide sequences. *Nucleic Acids Res* **32:** 11–16.

Lee, I.M., Tu, I.F., Yang, F.L., Ko, T.P., Liao, J.H., Lin, N.T., *et al.* (2017) Structural basis for fragmenting the exopolysaccharide of *Acinetobacter baumannii* by bacteriophage PhiAB6 tailspike protein. *Sci Rep* **7:** 42711.

Lin, N.-T., Chiou, P.-Y., Chang, K.-C., Chen, L.-K., and Lai, M.-J. (2010) Isolation and characterization of φAB2: a novel bacteriophage of *Acinetobacter baumannii. Res Microbiol* **161:** 308–314.

Lin, T.L., Hsieh, P.F., Huang, Y.T., Lee, W.C., Tsai, Y.T., Su, P.A., *et al.* (2014) Isolation of a bacteriophage and its depolymerase specific for K1 capsule of *Klebsiella pneumoniae*: implication in typing and treatment. *J Infect Dis* **210:** 1734–1744.

Majkowska-Skrobek, G., Łątka, A., Berisio, R., Maciejewska, B., Squeglia, F., Romano, M., *et al.* (2016) Capsule-targeting depolymerase, derived from *Klebsiella* KP36 phage, as a tool for the development of anti-virulent strategy. *Viruses* **8:** 324.

Marti, R., Zurfluh, K., Hagens, S., Pianezzi, J., Klumpp, J., and Loessner, M.J. (2013) Long tail fibres of the novel broad-host-range T-even bacteriophage S16 specifically recognize *Salmonella* OmpC. *Mol Microbiol* **87:** 818–834.

Meier-Kolthoff, J.P., Auch, A.F., Klenk, H.P., and Goker, M. (2013) Genome sequence-based species delimitation with confidence intervals and improved distance functions. *BMC Bioinf* **14:** 60.

Merabishvili, M., Vandenheuvel, D., Kropinski, A.M., Mast, J., De Vos, D., Verbeken, G., *et al.* (2014) Characterization of newly isolated lytic bacteriophages active against *Acinetobacter baumannii. PLoS One* **9:** e104853.

Migl, D.M. (2012). Expression, purification, and characterization of a polysaccharide depolymerase from *Acinetobacter baumannii* bacteriophage abauya1. An Honors Fellow Thesis. TX: Texas A&M University.

Mumm, I.P., Wood, T.L., Chamakura, K.R., and Kuty Everett, G.F. (2013) Complete genome of *Acinetobacter baumannii* Podophage Petty. *Genome Announc* **1:** pii e00850-13.

Nakar, D., and Gutnick, D.L. (2001) Analysis of the wee gene cluster responsible for the biosynthesis of the polymeric bioemulsifier from the oil-degrading strain *Acinetobacter lwoffii* RAG-1. *Microbiology* **147:** 1937–1946.

Naville, M., Ghuillot-Gaudeffroy, A., Marchais, A., and Gautheret, D. (2011) ARNold: a web tool for the prediction

of Rho-independent transcription terminators. *RNA Biol* **8:** 11–13.

Nemec, A., Krizova, L., Maixnerova, M., van der Reijden, T.J., Deschaght, P., Passet, V., *et al.* (2011) Genotypic and phenotypic characterization of the *Acinetobacter calcoaceticus-Acinetobacter baumannii* complex with the proposal of Acinetobacter pittii sp. nov. (formerly *Acinetobacter* genomic species 3) and *Acinetobacter nosocomialis* sp. nov. (formerly *Acinetobacter* genomic species 13TU). *Res Microbiol* **162:** 393–404.

Nemec, A., Krizova, L., Maixnerova, M., Sedo, O., Brisse, S., and Higgins, P.G. (2015) *Acinetobacter seifertii* sp. nov., a member of the *Acinetobacter calcoaceticus-Acinetobacter baumannii* complex isolated from human clinical specimens. *Int J Syst Evol Microbiol* **65:** 934–942.

Oliveira, H., Pinto, G., Oliveira, A., Oliveira, C., Faustino, M.A., Briers, Y., *et al.* (2016) Characterization and genome sequencing of a *Citrobacter freundii* phage CfP1 harboring a lysin active against multidrug-resistant isolates. *Appl Microbiol Biotechnol* **100:** 10543–10553.

Pan, Y.J., Lin, T.L., Chen, Y.H., Hsu, C.R., Hsieh, P.F., Wu, M.C., and Wang, J.T. (2013) Capsular types of *Klebsiella pneumoniae* revisited by wzc sequencing. *PLoS One* **8:** e80670.

Pedulla, M.L., Ford, M.E., Houtz, J.M., Karthikeyan, T., Wadsworth, C., Lewis, J.A., *et al.* (2003) Origins of highly mosaic mycobacteriophage genomes. *Cell* **113:** 171–182.

Pelkonen, S., Aalto, J., and Finne, J. (1992) Differential activities of bacteriophage depolymerase on bacterial polysaccharide: binding is essential but degradation is inhibitory in phage infection of K1-defective *Escherichia coli*. *J Bacteriol* **174:** 7757–7761.

Peng, Y., Leung, H.C., Yiu, S.M., and Chin, F.Y. (2012) IDBA-UD: a de novo assembler for single-cell and metagenomic sequencing data with highly uneven depth. *Bioinformatics* **28:** 1420–1428.

Pires, D.P., Oliveira, H., Melo, L.D., Sillankorva, S., and Azeredo, J. (2016) Bacteriophage-encoded depolymerases: their diversity and biotechnological applications. *Appl Microbiol Biotechnol* **100:** 2141–2151.

Popova, A.V., Lavysh, D.G., Klimuk, E.I., Edelstein, M.V., Bogun, A.G., Shneider, M.M., *et al.* (2017) Novel Fri1-like viruses infecting *Acinetobacter baumannii*-vB_AbaP_AS11 and vB_AbaP_AS12-characterization, comparative genomic analysis, and host-recognition strategy. *Viruses* **9:** 188.

Proctor, L., Fuhrman, J., and Ledbetter, M. (1988) Marine bacteriophages and bacterial mortality. *Eos* **69:** 1111–1112.

Rakhuba, D., Kolomiets, E., Szwajcer Dey, E., and Novik, G. (2010) Bacteriophage receptors, mechanisms of phage adsorption and penetration into host cell. *Polish J Microbiol* **59:** 145–155.

Rice, P., Longden, I., and Bleasby, A. (2000) EMBOSS: the European molecular biology open software suite. *Trends Genet* **16:** 276–277.

Rodriguez-Valera, F., Martin-Cuadrado, A.-B., Rodriguez-Brito, B., Pasic, L., Thingstad, T.F., Rohwer, F., and Mira, A. (2009) Explaining microbial population genomics through phage predation. *Nat Rev Microbiol* **7:** 828–836.

Rossello-Mora, R., and Amann, R. (2015) Past and future species definitions for *Bacteria* and *Archaea*. *Syst Appl Microbiol* **38:** 209–216.

Russo, T.A., Luke, N.R., Beanan, J.M., Olson, R., Sauberan, S.L., MacDonald, U., *et al.* (2010) The K1 capsular polysaccharide of *Acinetobacter baumannii* strain 307-0294 is a major virulence factor. *Infect Immun* **78:** 3993–4000.

Sambrook, J., and Russel, D. (2001). *Molecular Cloning: A Laboratory Manual.* Cold Spring Harbor, NY: Cold Spring Harbor Labroratory Press.

Samson, J.E., Magadan, A.H., Sabri, M., and Moineau, S. (2013) Revenge of the phages: defeating bacterial defences. *Nat Rev Microbiol* **11:** 675–687.

Schattner, P., Brooks, A.N., and Lowe, T.M. (2005) The tRNAscan-SE, snoscan and snoGPS web servers for the detection of tRNAs and snoRNAs. *Nucleic Acids Res* **33:** W686–W689.

Scholl, D., Adhya, S., and Merril, C. (2005) Escherichia coli K1's capsule is a barrier to bacteriophage T7. *Appl Environ Microbiol* **71:** 4872–4874.

Scorpio, A., Chabot, D.J., Day, W.A., O'Brien, D.K., Vietri, N.J., Itoh, Y., *et al.* (2007) Poly-gamma-glutamate capsule-degrading enzyme treatment enhances phagocytosis and killing of encapsulated *Bacillus anthracis*. *Antimicrobial Agents Chemother* **51:** 215–222.

Shashkov, A.S., Kenyon, J.J., Arbatsky, N.P., Shneider, M.M., Popova, A.V., Miroshnikov, K.A., *et al.* (2015a) Structures of three different neutral polysaccharides of *Acinetobacter baumannii*, NIPH190, NIPH201, and NIPH615, assigned to K30, K45, and K48 capsule types, respectively, based on capsule biosynthesis gene clusters. *Carbohydr Res* **417:** 81–88.

Shashkov, A.S., Shneider, M.M., Senchenkova, S.N., Popova, A.V., Nikitina, A.S., Babenko, V.V., *et al.* (2015b) Structure of the capsular polysaccharide of *Acinetobacter baumannii* 1053 having the KL91 capsule biosynthesis gene locus. *Carbohydr Res* **404:** 79–82.

Shashkov, A.S., Kenyon, J.J., Arbatsky, N.P., Shneider, M.M., Popova, A.V., Miroshnikov, K.A., *et al.* (2016a) Related structures of neutral capsular polysaccharides of *Acinetobacter baumannii* isolates that carry related capsule gene clusters KL43, KL47, and KL88. *Carbohydr Res* **435:** 173–179.

Shashkov, A.S., Kenyon, J.J., Senchenkova, S.N., Shneider, M.M., Popova, A.V., Arbatsky, N.P., *et al.* (2016b) *Acinetobacter baumannii* K27 and K44 capsular polysaccharides have the same K unit but different structures due to the presence of distinct wzy genes in otherwise closely related K gene clusters. *Glycobiology* **26:** 501–508.

Shin, H., Lee, J.-H., Kim, H., Choi, Y., Heu, S., Ryu, S., and Hensel, M. (2012) Receptor diversity and host interaction of bacteriophages infecting *Salmonella* enterica serovar Typhimurium. *PLoS One* **7:** e43392.

Singh, S.K., Bharati, A.P., Singh, N., Pandey, P., Joshi, P., Singh, K., *et al.* (2014) The prophage-encoded hyaluronate lyase has broad substrate specificity and is regulated by the N-terminal domain. *J Biol Chem* **289:** 35225–35236.

Soding, J., Biegert, A., and Lupas, A.N. (2005) The HHpred interactive server for protein homology detection and structure prediction. *Nucleic Acids Res* **33:** W244–W248.

Stummeyer, K., Schwarzer, D., Claus, H., Vogel, U., Gerardy-Schahn, R., and Muhlenhoff, M. (2006) Evolution of bacteriophages infecting encapsulated bacteria: lessons from *Escherichia coli* K1-specific phages. *Mol Microbiol* **60:** 1123–1135.

Sullivan, M.J., Petty, N.K., and Beatson, S.A. (2011) Easyfig: a genome comparison visualizer. *Bioinformatics* **27:** 1009–1010.

Suttle, C. (2007) Marine viruses - major players in the global ecosystem. *Nat Rev Microbiol* **5:** 801–812.

Taylor, N.M., Prokhorov, N.S., Guerrero-Ferreira, R.C., Shneider, M.M., Browning, C., Goldie, K.N., *et al.* (2016) Structure of the T4 baseplate and its function in triggering sheath contraction. *Nature* **533:** 346–352.

Thompson, J.E., Pourhossein, M., Waterhouse, A., Hudson, T., Goldrick, M., Derrick, J.P., and Roberts, I.S. (2010) The K5 lyase KflA combines a viral tail spike structure with a bacterial polysaccharide lyase mechanism. *J Biol Chem* **285:** 23963–23969.

Touchon, M., Cury, J., Yoon, E.J., Krizova, L., Cerqueira, G.C., Murphy, C., *et al.* (2014) The genomic diversification of the whole *Acinetobacter* genus: origins, mechanisms, and consequences. *Genome Biol Evol* **6:** 2866–2882.

Trimble, W.L., Keegan, K.P., D'Souza, M., Wilke, A., Wilkening, J., Gilbert, J., and Meyer, F. (2012) Short-read reading-frame predictors are not created equal: sequence error causes loss of signal. *BMC Bioinf* **13:** 183.

Tusnady, G.E., and Simon, I. (2001) The HMMTOP transmembrane topology prediction server. *Bioinformatics* **17:** 849–850.

Ventola, C.L. (2015) The antibiotic resistance crisis: Part 1: Causes and threats. *Pharm Ther* **40:** 277–283.

Vinga, I., Baptista, C., Auzat, I., Petipas, I., Lurz, R., Tavares, P., *et al.* (2012) Role of bacteriophage SPP1 tail spike protein gp21 on host cell receptor binding and trigger of phage DNA ejection. *Mol Microbiol* **83:** 289–303.

Whitfield, C. (2006) Biosynthesis and assembly of capsular polysaccharides in *Escherichia coli*. *Annu Rev Biochem* **75:** 39–68.

Whitfield, C., and Roberts, I.S. (1999) Structure, assembly and regulation of expression of capsules in *Escherichia coli*. *Mol Microbiol* **31:** 1307–1319.

Xia, G., Corrigan, R.M., Winstel, V., Goerke, C., Grundling, A., and Peschel, A. (2011) Wall teichoic acid-dependent adsorption of staphylococcal siphovirus and myovirus. *J Bacteriol* **193:** 4006–4009.

Zafar, N., Mazumder, R., and Seto, D. (2002) CoreGenes: A computational tool for identifying and cataloging "core" genes in a set of small genomes. *BMC Bioinf* **3:** 12.

Supporting information

Additional Supporting Information may be found in the online version of this article at the publisher's web-site:

Table S1. Phage lytic spectra. Susceptibility of strains from all species that currently belong to the **A. calcoaceticus-A. baumannii** complex (*A. baumannii*, *A. calcoaceticus*, *A. pittii*, *A. seifertii*, *A. nosocomialis*, and *A. dijkshoorniae*) to the 12 isolated phages. Green rectangles mean productive lysis and yellow rectangles mean events of lysis from without. The relative EOP was calculated as the titre of the phage (PFU/ml) for each isolate divided by the titre for the propagating host and recorded as high (≥ 0.5) or low (< 0.5).

Table S2. Adsorption rates of the isolated phages to the infected *A. calcoaceticus-A. baumannii* complex strains. Bold symbolizes the propagation host. Statistical differences

determined by Student's *t* test with a 99% confidence level are presented.

Table S3. Features of phage P1 predicted CDSs. For each CDS the transcription start and stop position, and the coding strand is given. At protein level the corresponding gene product size molecular weight and pI as well as the homolog predicted function homology, values and motifs are shown.

Table S4. Features of phage P2 predicted CDSs. For each CDS the transcription start and stop position, and the coding strand is given. At protein level the corresponding gene product size molecular weight and pI as well as the homolog predicted function, homology values and motifs are shown.

Table S5. Features of phage B1 predicted CDSs. For each CDS the transcription start and stop position, and the coding strand is given. At protein level the corresponding gene product size molecular weight and pI as well as the homolog predicted function homology, values and motifs are shown.

Table S6. Features of phage B3 predicted CDSs. For each CDS the transcription start and stop position, and the coding strand is given. At protein level the corresponding gene product size molecular weight and pI as well as the homolog predicted function, homology values and motifs are shown.

Table S7. Features of phage B5 predicted CDSs. For each CDS the transcription start and stop position, and the coding strand is given. At protein level the corresponding gene product size molecular weight and pI as well as the homolog predicted function homology, values and motifs are shown.

Table S8. Comparative nucleotide analysis of phages infecting strains of the *A. calcoaceticus-A. baumannii* complex. The newly isolated phages P1 (MF033350), P2 (MF033351), B1 (MF033347), B3 (MF033348) and B5 (MF033349) were compared to each other and to all other sequenced *Acinetobacter* podoviruses in NCBI, namely, *A. baumannii* phages Abp1 (NC_021316), phiAB1 (NC_028675), PD-AB9 (NC_028679), PD-6A3 (NC_028684), Fri1 (NC_028848), phiAB6 (NC_031086), AS11 (KY268296), AS12 (KY268295), WCHABP5 (KY888680), IME200 (NC_028987), SH-Ab 15519 (KY082667), Petty (NC_023570) and Acibel007 (NC_025457), using EMBOSS Stretcher. Bold numbers indicate significant homologies higher than 80%.

Table S9. Strains of the *A. calcoaceticus-A. baumannii* complex used in this study. ANC and NIPH, strain designations used by the Laboratory of Bacterial Genetics, Prague, Czech Republic; ATCC, American Type Culture Collection, Manassas, VA; CCUG, Culture Collection, University of Göteborg, Sweden; CIP, Collection de l'Institut Pasteur, Institut Pasteur, Paris, France; LMG, Bacteria Collection, Laboratorium voor Microbiologie Gent, Gent, Belgium; LUH and RUH, strain designations used by L. Dijkshoorn, the Leiden Medical Center, the Netherlands. All clinical strains were of human origin. Sequence types (ST) contain the concatenated sequences of the seven genes used in the multilocus sequence analysis (MLSA) and are numbered according to the Pasteur MLSA scheme (http://pubmlst.org/abaumannii. Whole-genome sequences are indicated by their DDBJ/ENA/GenBank accession numbers.

Table S10. Allocation of the capsular genes of the *A. calcoaceticus-A. baumannii* complex strains with genome

sequences used in this study. KL – K-locus of a determined capsule structure (K-type); n.a. – capsule structure is not available.

Fig. S1. Electron micrographs of negatively stained *Acinetobacter* phages. All isolated phages were classified into the *Podoviridae* family morphotype C. Scale bars represent 100 nm.

Fig. S2. Pattern of K locus variation of *A. calcoaceticus-A. baumannii* complex strains. Genes of each cluster are presented in map order and with a colour scheme for specific functions. Genes within a column with the same colour have the same sequence. Loci can be accessible by the GenBank entries and the positions listed in Supporting Information Table S10. Indicated at the bottom are other known *A. baumannii* strains, ATCC 17978 (CP000521), 28 (KU215659.1) and 4190 (KT266827) mentioned in the literature, which are hosts for phages phiAB2, Fri1/AS11 and AS12 respectively, whose sequences were retrieved from Genbank accession numbers indicated. Unk – gene with unknown function; Trsp – transposase. ItrB2* are genes interrupted by transposases. pgt1* are genes interrupted by a ISAba25-like insertion sequence.